Invited Paper

Silicon "plasmonics" and optical field concentration at nanometer scale.

Vergeles S.S.[a,b] and Sarychev A.K.[b,c]

[a] Institute for Theoretical Physics of RAS, Chernogolovka, 142432, Russia
[b] Moscow Institute of Physics and Technology, Dolgoprudny, 141700, Russia
[c] Institute for Theoretical and Applied Electrodynamics, Moscow 125412, Russia

ABSTRACT

Concentration of light into nanospots is greatly beneficial for heat assisted magnetic recording, biomedical imaging and sensing, nanolasing, etc. We propose novel, all dielectric near field transducers, which allow focusing light into a hot spot, much smaller than the wavelength without significant dissipative loss. Therefore, the detrimental thermal effects in heat assisted recording can be significantly reduced opening new venue in the magnetic recording. In the proposed transducer electric field concentrates at the apex of the dielectric tip attached to the resonator. Thus the electric field excited in the dielectric resonator is further amplified and concentrated due to the dipole polarization of the tip.

1. INTRODUCTION

Concentration of the light into nanospots much smaller than the wavelength is the crucial problem for the applications such as biomedical imaging and sensing, optical microscopy with single-molecule resolution,[1] heat assisted magnetic recording (HAMR),[2] QED,[3] nanolasing, etc. Until now, metal plasmonic nanoantennae or near field transducers (NFT) have been used for this purpose.[4,5] We propose novel, all - dielectric class of NFTs, which allow focusing light into a hot spot, much smaller than the wavelength without significant dissipative optical loss characteristic to the metal NFTs. Therefore, the detrimental thermal effects in HAMR can be significantly reduced opening new venue in the magnetic recording.[6–8] We consider an NFT in the form of the pumped resonator, where the electric field concentrates at the apex of a tip attached to the resonator at a proper point as it is shown in Fig. 1a.

2. MAGNETIC DIPOLE FIELD IN THE RESONATOR

The electromagnetic field is pumped in the magnetic Mie dipole resonances excited in the dielectric sphere of the radius a.[9] The sphere with permittivity $\varepsilon = n^2$ is placed in the origin of the coordinates. The permittivity of the outer space is chosen to be equal to one. The electromagnetic field oscillates with resonance frequency ω, wave vector $k = \omega/c$. We use the spherical symmetry of the problem to introduce the electric vector potential for the inside field $A_z^{\rm in} = -E_0 \sin(u)/\left[knuf(u_a)\right]$ directed along z axis, where the dimensionless coordinate $u = knr$, $u_a = kna$, and the function $f(u) = (\sin u - u\cos u)/u^2$; $r = \sqrt{x^2+y^2+z^2}$. It is convenient to introduce spherical coordinates $\{r, \theta, \varphi\}$ with z axis perpendicular to the plane of the Figs. 1 and 2. The electric and magnetic fields inside the sphere are

$$\mathbf{E}^{\rm in}(r,\theta,\varphi) = {\rm curl}\mathbf{A}^{\rm in} = E_0\left[f(u)/f(u_a)\right]\sin\theta\,\{0,0,1\}\,,\quad \mathbf{H}^{\rm in}(r,\theta,\varphi) = {\rm curl}\mathbf{E}^{\rm in}/ik. \tag{1}$$

The outside electromagnetic field is given by the vector potential $A_z^{\rm e} = E_0\, u_a^2 \exp\left[ik(r-a)\right]/\left[ku(n-iu_a)\right]$, where the radiation boundary condition is imposed at the infinity:

$$\mathbf{E}^{\rm e}(r,\theta,\varphi) = {\rm curl}\mathbf{A}^{\rm e} = E_0\exp\left[ik(r-a)\right]\frac{u_a^2(n-iu)}{u^2(n-iu_a)}\sin\theta\;\{0,0,1\}\,,\quad \mathbf{H}^{\rm e} = \frac{{\rm curl}\mathbf{E}^{\rm e}}{ik}. \tag{2}$$

Further author information: Send correspondence to A.K.S., E-mail: sarychev_andrey@yahoo.com, Telephone: +7 926 471 4000

Metamaterials, Metadevices, and Metasystems 2015, edited by Nader Engheta, Mikhail A. Noginov, Nikolay I. Zheludev, Proc. of SPIE Vol. 9544, 954415
 · doi: 10.1117/12.2187532

That is electric field in the magnetic dipole resonance circulate around z axis, which is perpendicular to the figure plane.

The vector potentials $\mathbf{A}^{\rm in}$ and $\mathbf{A}^{\rm e}$ are chosen in such a way that the boundary conditions $E^{\rm in}_{\varphi}(a) = E^{\rm e}_{\varphi}(a) = E_0$ and $H^{\rm in}_{r}(a) = H^{\rm e}_{r}(a)$ automatically accomplish. The third boundary condition $H^{\rm in}_{\theta}(a) = H^{\rm e}_{\theta}(a)$ gives the equation for the resonance frequencies

$$u_a \cos u_a + \left(n^2 - 1 - in\, u_a\right) \sin u_a = 0. \tag{3}$$

Substituting here the silicon red–infrared parameters $n^2 = \varepsilon_{Si} \simeq 15$[10,11] we obtain the roots $u_1 \approx 3.01 - 0.1i$, $u_2 \approx 6.16 - 0.19i$, $u_3 \approx 9.33 - 0.23\,i$, etc.

It follows from Eq. (3) that the first, second and third magnetic dipole resonances take place at the wavelength $\lambda = 900\,nm$ for the silicon micro particles with radii $a \simeq 111$, 228, and $345\,nm$ correspondingly. The Q factors for the resonances equal to $Q \cong 14.5, 15.9$ and 20.5 correspondingly. We use the electromagnetic field of the first resonance to effectively illuminate the tip. For the refractive index $n \gg 1$ the resonance frequency and Q factor estimate from Eq. (3) as $u_m = \pi m \left(1 - n^{-2} - i\pi m n^{-3}\right)$ and $Q_m = n\left(n^2 - 1\right)/(2m\pi)$, $m = 1, 2 \ldots$, where the imaginary part stands for the radiative loss assuming that the absorption is small. Note the silicon refractive index is not large enough and the analytical equations give semi-qualitative esteem only.

Our computer simulations, presented in Figs. 1,2, we performed in FEMLAB environment. The whole system including tip, resonator, and waveguide have been surrounded by perfect matching layer (PML) sphere, which radius is about $10a$. The waveguide port, which is placed near the intersection of the dielectric waveguide and the PML sphere, is used to launch the em wave in the waveguide, which in turn pumps the spherical resonator. The length of the tapered waveguide waist was optimized in order to achieve maximum field intensity inside the resonator. The maximum of the resonator field corresponds to the minimum amplitude of the reflected wave in the waveguide.

Calculations are done for the silicon resonator operating in the red and near infrared spectral range ($\lambda > 800\,nm$) where the permittivity of Si $\varepsilon \simeq 15$ (see e.g.[10,11]); the ohmic loss is neglected as being much smaller than the radiation loss. We assume, for simplicity, that the permittivity of the surrounding space is one. The external field ($r > a$), which excites the tip, can be rewritten as

$$E^e_x = E^{\rm e}_{\varphi} \sin\varphi, \quad E^e_y = -E^{\rm e}_{\varphi} \cos\varphi \tag{4}$$

where the amplitude $E^{\rm e}_{\varphi}$ (see Eq. 2) is determined by em energy pumped in the resonator through the waveguide shown in Fig. 1.

3. POLARIZATION OF A PROLATE BODY PLACED IN NONUNIFORM ELECTROMAGNETIC (EM) FIELD

In the proposed NFT the dielectric beak is attached to the spherical resonator (Fig. 1). The nonuniform resonator field, given by Eqs. (2),(4), excites the beak. We consider now one of a basic nanophotonics problem, namely, the field distribution inside a prolate body of rotation, which is placed in a nonuniform em field. The axis of the body of rotation is chosen as "y" axis. That is the body is a cylinder, which radius r depends on the coordinate y. We find the internal electric field in the much elongated cylinder of the length $2b \gg r$. The maximum radius $\max[r(y)] \equiv g \ll b$, and the body is assumed to be rather smooth, that is $\mathrm{d}r(y)/\mathrm{d}y \ll 1$. The end points of the body are placed at $y = \pm b$, corresponding to its length $2b$. For example, the radius r of the elliptic cylinder varies as

$$r(y) = g\sqrt{1 - (y/b)^2}, \tag{5}$$

where $b \gg g$ are semi-axes.

The cylinder is excited by the longitudinal field $E^{\rm e}(y)$ directed along y axis. The material of the cylinder is characterized by permittivity $\varepsilon = n^2$ or conductivity $\sigma \equiv -i\omega(\varepsilon - 1)/4\pi$. Full electric field $E^b(y)$ is the sum of the external field and the field induced by the electric current and charge

$$E^b(y) \;=\; E^e(y) - \frac{\mathrm{d}\Phi(y)}{\mathrm{d}y} + ikA_y(y), \tag{6}$$

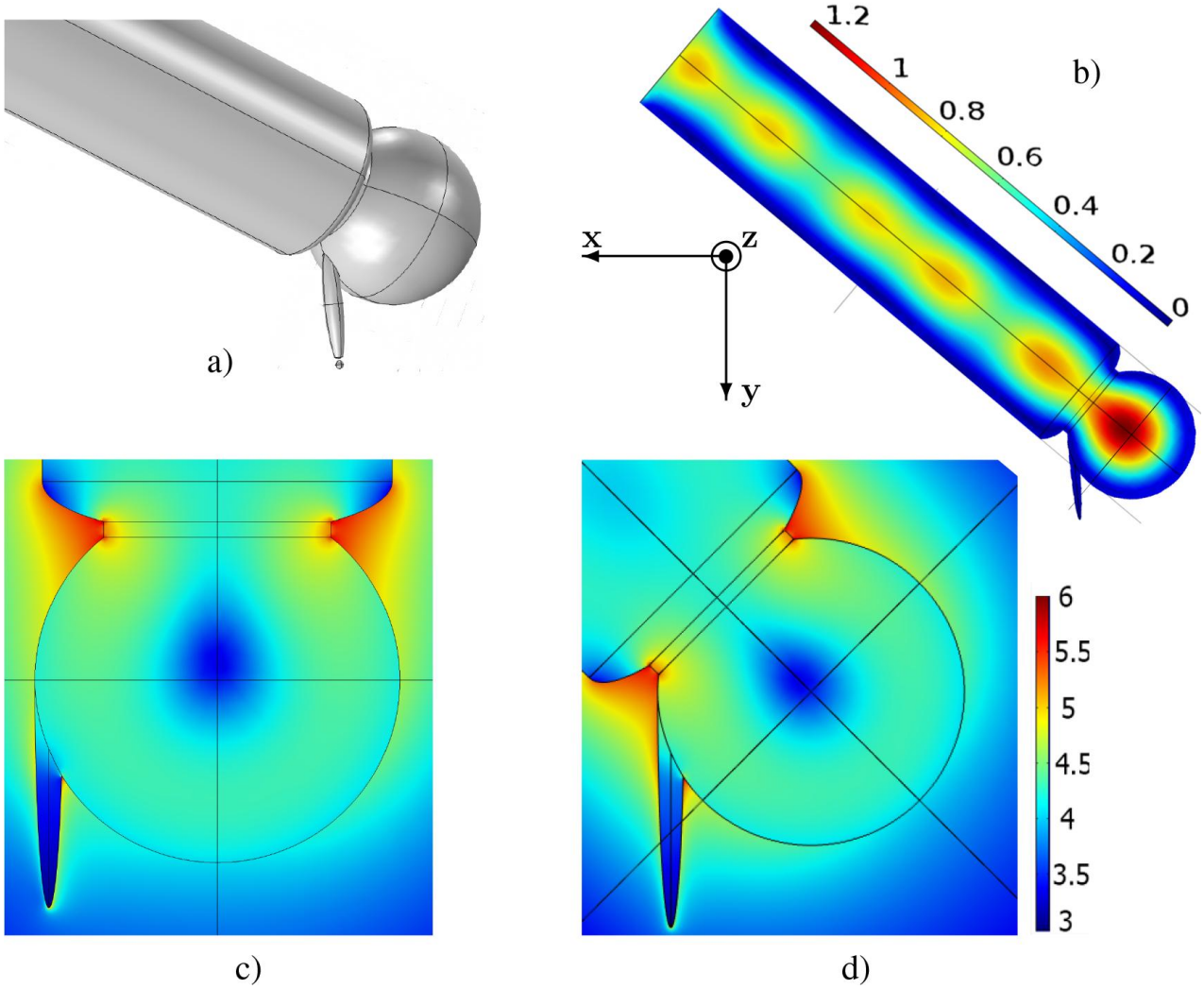

Figure 1. a) NFT consisting of cylindrical waveguide (radius ρ), spherical resonator (radius a) and prolate ellipsoidal nanotip; the diameter $5\,nm$ of the nanoparticle, hanging bellow the apex, corresponds to the area of the electric field concentration; b) numerical simulation in FEMLAB environment of the magnetic field $|H|$ [A/m], which is pumped in the resonator through the waveguide ($\rho = 107$, $a = 111\,nm$, $\lambda = 900\,nm$). c) Electric field $\ln|E|$ [V/m] excites the tip of length $b = 130\,nm$ and small semi-axis $g = 10\,nm$; vertical waveguide orientation; d) the same but waveguide is inclined.

where Φ and A_y are scalar and vector potentials; $k = \omega/c$. The transversal field, induced by the current and charge, is neglected since we assume $\mathrm{d}r(y)/\mathrm{d}y \ll 1$. Then the electric current is given by the Ohm law $J(y) = \pi r^2 f(y)\sigma E^b(y)$; the correction for the skin effect equals to $f(y) = 2J_1(u)/u$, where $u = nkr(y)$ and J_1 is the 1^{st} Bessel function. The electric potential Φ is produced by the charge, which is always distributed over the surface of the cylinder. Let $q(y)$ be the linear density of the charge, then the potential at the axis "y" is given by the integral

$$\Phi(y) = \int_{-b}^{b} \frac{e^{ik|y-y'|}\, q(y')\,\mathrm{d}y'}{\sqrt{(y-y')^2 + r(y')^2}}. \tag{7}$$

The most important singular part of the electric potential $\Phi(y)$ can be extract from the Eq. (7) in the following

way

$$\Phi(y) \approx q(y) \int_{-b}^{b} \frac{\mathrm{d}y'}{\sqrt{(y-y')^2 + r(y')^2}} + \int_{-b}^{b} \frac{\left[q(y')e^{ik|y-y'|} - q(y)\right] \mathrm{d}y'}{\sqrt{(y-y')^2 + r(y')^2}} \equiv \Phi_0(y) + \Phi_1(y) \tag{8}$$

To solve the first integral note that the term $r(y')^2 < g^2$ in the square root is only important for $|y - y'| < g$. We replace $r(y')^2$ by $r(y)^2$ since it is assumed that $\mathrm{d}r(y)/\mathrm{d}y \ll 1$:

$$\Phi_0(y) \approx q(y) \log\left(\frac{\sqrt{(b+y)^2 + r(y)^2} + b + y}{\sqrt{(b-y)^2 + r(y)^2} - b + y}\right) \approx \frac{q(y)}{C(y)}; \quad \frac{1}{C(y)} = \ln\frac{b^2 - y^2}{r^2(y)} \gg 1. \tag{9}$$

Thus the electric potential linearly depends on the charge density in the logarithmic approximation. The integral for potential $\Phi_1(y)$ in Eq. (8) has no singularity at $y = y'$. Therefore the potential $\Phi_1(y)$ gives only small correction to $\Phi_0(y)$. Yet, Φ_1 can be important when $b \geq \lambda$ since the phase of Φ_1 is shifted in respect to the charge $q(y)$ and, therefore, $\Phi_1(y)$ gives the radiation loss.

Using the same approach we obtain the vector potential $A_y(y) \approx L(y)J(y)/c$, where $L(y) = C(y)^{-1} = \ln\left[(b^2 - y^2)/r^2(y)\right]$, is the linear inductance, c – speed of light. We substitute the potentials Φ_0 and A_y in the Ohm law, use the charge conservation $i\omega q = \mathrm{d}J/\mathrm{d}y$ and obtain close equation for the electric current

$$J(y) = \pi r^2 f(y)\sigma \left[E^e(y) - \frac{1}{i\omega}\frac{\mathrm{d}}{\mathrm{d}y}\frac{1}{C(y)}\frac{\mathrm{d}}{\mathrm{d}y}J(y) + ik\frac{L(y)}{c}J(y)\right], \quad J(\pm b) = 0. \tag{10}$$

There is no problem to solve the above equation numerically and find the current J and internal field $E^b = J/(\pi r^2 f(y)\sigma)$ for any distribution of the external field $E^e(y)$. Note that in the case of strong skin effect ($\mathrm{Re}\,\sigma \to \infty$) the expression in the square brackets in r.h.s. Eq. (10) vanishes, which corresponds to the well known antenna equation.[12,13]

There is very important particular case of the prolate ellipsoid, when the local radius $r(y)$ is given by Eq. (5), and, therefore, the capacity and inductance do not depend on the position: $C = 1/L = 1/\left[2\ln(b/g)\right]$. We consider rather small ellipsoid $b \ll \lambda$ and neglect, for simplicity, the skin effect and inductance. Then Eq. (10) takes the form of the hypergeometric equation

$$(1 - y_1)\, y_1 \frac{\mathrm{d}^2 E^b}{\mathrm{d}y_1^2} + 2\,(1 - 2y_1)\,\frac{\mathrm{d}E^b}{\mathrm{d}y_1} - (2 + D_0)\,E^b + D_0 E^e(y_1) = 0, \tag{11}$$

where we use the dimensionless coordinate $y_1 = (1 - y/b)/2$, $D_0 = 2/\left[n_y(\varepsilon - 1)\right]$, depolarization coefficient $n_y = (g/b)^2 \ln(2b/g)$. The solution of Eq. (11), which is regular for $0 \geq y_1 \leq 1$, is given by the following equation

$$E^b(y_1) = D_0^2 \left[\int_0^{y_1} (1-t)t\, W(y_1, t) E^e(t)\, dt + Y(y_1)\frac{\sin(\alpha\pi)}{\pi}\int_0^1 (1-t)tY(t)\, E^e(1-t)dt\right], \tag{12}$$

where the Green function equals to

$$W(y_1, t) = Y(y_1)V(t) - Y(t)V(y_1), \tag{13}$$

where $Y(y)$ and $V(y)$ are two independent solutions of the homogeneous equation (11) when $E^e = 0$. The regular solution

$$Y(y) = \frac{\sin(\pi\alpha))}{\pi(\alpha - 2)(\alpha - 1)} \sum_{n=0}^{\infty} \frac{\Gamma(n - \alpha + 3)\Gamma(n + \alpha)}{n!(n+1)!} y^n = F(\alpha, 3 - \alpha, 2, y), \tag{14}$$

is the standard hypergeometric function, where $\alpha = \left(3 + \sqrt{1 - 4D_0}\right)/2$. The function $V(y)$ in Eq. (13) is the second solution of the homogeneous equation (11), which we choose in the following form

$$V(y) = \frac{1}{D_0 y} + Y(y)(f_0 + \log y) + \phi(y) \tag{15}$$

where $f_0 = 1 - H_{2-\alpha} - H_{\alpha-1}$, H_n is the Harmonic Number of the order n; the function

$$\phi(y) = \sum_n^{\infty} \left[H_{-\alpha+n+2} + \psi(\alpha+n) - 2H_n - \frac{1}{n+1} + \gamma \right] y^n, \tag{16}$$

where γ is the Euler constant, $\psi(y) = \mathrm{d}\ln\Gamma(y)/\mathrm{d}y$ is the polygamma function. The sum for $\phi(y)$ absolutely converges for $|y| < 1$.

The equation for the internal field E^b is much simplified when the external field expands in the series $E^e = \sum_{m=0}^{m=n} E_m y_1^m$. Then the internal field in the tip is the also polynomial $E^b = D_0 \sum_{m=0}^{m=n} E_m W_m$, where the polynomial

$$W_m(y_1) = \frac{m!\,(m+1)!}{\Gamma(4-a+m)\Gamma(1+a+m)} \sum_{k=0}^{k=m} \frac{\Gamma(3-a+k)\Gamma(a+k)}{k!\,(k+1)!} y_1^k. \tag{17}$$

For example, let us suppose that the external field approximates by third order polynomial $E^b(y_1) = E_0^b + E_1^b\, y_1 + E_2^b\, y_1^2$ then Eq. (17) gives the internal field in the following form:

$$E^b(y_1) = \frac{D_0}{D_0+2} \left[E_0^b + E_1^b \frac{2 + (D_0+2)y_1}{D_0+6} + E_2^b \frac{12 + y_1(D_0+2)(6 + y_1(D_0+6))}{(D_0+6)(D_0+12)} \right]. \tag{18}$$

In the case of the much elongated ellipsoid, when $D_0 \gg 1$, the internal nonuniform field $E^b(y)$ follows the external nonuniform field $E^b(y) \approx E^e(y)$. Recall that above results have been obtained with so-called logarithmic accuracy: we assume that not only $b/g \gg 1$ but also $\ln(b/g) \gg 1$.

4. FIELD ENHANCEMENT AT THE APEX OF THE DIELECTRIC TIP

We consider the tip in Fig. 1 in the form of a prolate ellipsoid with semiaxes b and $g \ll b$. Note that the field in a rectangular nanocelynder is less enhanced, as it is shown in Fig. 2b (black curve). The tip is placed in the equatorial "x, y" plane ($\theta = \pi/2$) with its longer axis parallel to y - axis as it is shown in Fig. 1. The center of the tip is located on x - axis at the distance d from the center. For the thin tip $g \ll a$, the inside field $\left\{E_x^b, E_y^b\right\}$ can be estimated as the field in a prolate ellipsoid that is placed in the external field given by Eq. (1). The field enhancement at the apex of the sharp dielectric tip can be understood as follows:[14] the external driving field, polarized along tip axis, drives the bounded electrons periodically forth and back along the tip shaft with the same frequency as the exciting field. Because of the small surface area near the tip apex the uniform displacement of the bounded electrons gives rise of a huge surface charge accumulation at the tip apex. These charges generate a secondary field which is seen in Fig. 1 as enhanced field at the tip apex. The electric charges $q(y)$ are induced on the surface of the tip by the external inhomogeneous field $E_y^e(y)$. When the external electric field $E_y^e(y)$ is expanded in a series $E_y^e = E_0^e + E_1^e y_1 + E_2^e y_1^2 + \ldots$, $y_1 = (1 - y/b)/2$, the field in the tip is also polynomial, as it follows from Eq. (18). The internal field, extrapolated to the apex, equals to

$$E_y^b(b) = \frac{D_0}{D_0+2} \left[E_0^e + \frac{2E_1^e}{D_0+6} + \frac{12E_2^e}{(D_0+6)(D_0+12)} \cdots \right], \tag{19}$$

For the elongated tip, where $D_0 \gg 1$, the internal field close to the applied $E_y^b \simeq E_y^e$. The field, which is perpendicular to the tip shaft, approximates as $E_x^b = E_x^e/[1 + n_x(\varepsilon - 1)]$, where the transversal depolarization factor equals to $n_x \cong 1/2$ for $g \ll b$. The electric field intensity I_s at the surface of the tip $I_s(y) = \varepsilon^2 \left|\mathbf{E}^b \cdot \mathbf{n}^b\right|^2 + \left|\mathbf{E}^b - \left(\mathbf{E}^b \cdot \mathbf{n}^b\right)\right|^2$ is shown in Fig. 2a, where $\mathbf{n}^b$ is normal to the surface. The field intensity at the apex of the tip estimates from Eqs. (4) and (19) as

$$I_s(b) \simeq |E_0|^2 \frac{a^4 \left(d^2\varepsilon^2 + b^2\right)\left((b^2+d^2)k^2 + 1\right)}{\left((ak)^2+1\right)\left(b^2+d^2\right)^3}, \tag{20}$$

where E_0 (see Eq. 4) is the field at the surface of the resonator and $k \simeq \pi/(na)$ is the resonance wavevector. For $n \gg 1$ the tip intensity $I_s(b)$ achieves maximum value

$$I_m \simeq |E_0|^2 \varepsilon^2 (\pi a^2/b^2)^2 (a^2/(\pi^2 b^2) + \varepsilon^{-1})(a^2/b^2 + 1)^{-3} \tag{21}$$

for $d \approx a$. The maximum intensity I_m estimates for the silicon resonator with the resonance wavelength $\lambda_r = 900\,nm$, ($\varepsilon \cong 15$) and geometric parameters $a = 111\,nm$, $b = 150\,nm$, $g = 10\,nm$ as $I_m \approx 20|E_0|^2$ (see Fig. 1c). The cascade enhancement of the electric field is being achieved: first, there is a resonance in the dielectric resonator, then the resonant field is further amplified due to the tip polarization (c.f.[15]). The electric field just outside the apex approximates as

$$I(y_2) = I_m \left[(2y_2/\varepsilon + 1) \,/\, (2y_2 + 1)\right]^2, \tag{22}$$

where $y_2 = (y - b)/R > 0$ and $R = g^2/b$ is the curvature of the tip at the apex. Electric field concentrates in the sub-wave volume that scale $\sim R^3 \ll g^3 \ll \lambda^3$ (Fig. 2b) is of the same order or even smaller than in plasmonic nanoantennae.[16]

The spherical silicon resonator, where the tip is protrude from, is pumped through the dielectric waveguide. Hereby, we deliver the electric field to the apex without widespread exposure in contrast to ANSOM. We consider the silicon cylindrical waveguide attached to the resonator as it is shown in Fig. 1d. To effectively pump the resonator, we should match the impedances of the resonator Z_r and waveguide Z_w. The input impedance Z_r is defined by the equation $[\mathbf{n}^r \times [\mathbf{n}^r \times \mathbf{E}_0]] = Z_r\,[\mathbf{n}^r \times \mathbf{H}_0]$, where $\mathbf{E}_0$ and $\mathbf{H}_0$ are the fields at the surface of the resonator given by Eq. (2) and $\mathbf{n}^r = -\mathbf{r}/r$ is the inward normal. At the magnetic resonance Z_r, remains the same for any point at the surface and approximates as $Z_r \approx 0.4 + 1.1\,i$ for $\lambda_r = 900\,nm$.

When the radius ρ of the dielectric waveguide is sufficiently large $\rho k n > 1$, the electromagnetic wave is well confined inside. Then the waveguide impedance, calculated from the equation $[\mathbf{n}^r \times [\mathbf{n}^r \times \mathbf{E}^w]] = Z_w\,[\mathbf{n}^r \times \mathbf{H}^w]$, takes the value $Z_w = n^{-1} \approx 0.252 \neq Z_r$. There is no matching between the waveguide and the resonator so that the reflectance $R_w = |(Z_w - Z_r)/(Z_w + Z_r)|^2 > 0.75$. To decrease the reflectance R_w between the waveguide and the resonator we decrease the waveguide radius. When the waveguide radius ρ decreases below the critical value

$$\rho_c = \nu_{01}/(k\sqrt{n^2 - 1}), \tag{23}$$

where ν_{01} is the first zero of the Bessel function J_0, the phase constant estimates as

$$q \simeq k\sqrt{1 + \frac{4}{(\rho k)^2}\exp\left[-\left(n^2 + 1\right) J_0\left(p\right) / \left(pJ_1\left(p\right)\right) - 2\gamma\right]}, \tag{24}$$

where γ is Euler constant, $p = \rho k\sqrt{n^2 - 1}$, $J_0(p)$ and $J_1(p)$ are the Bessel functions. Since q is exponentially close to k the electromagnetic field spills out of the waveguide and spreads over all the space. In this case, the waveguide impedance Z_w depends on the coordinates and takes almost any values in the plane perpendicular to the waveguide axis. We optimize the position of the resonator in respect to the waveguide to achieve maximum field in the resonator. For $\lambda = 900\,nm$ we match the resonator and the waveguide by introducing a tapered waveguide waist, with a radius $\rho_w = 65\,nm < \rho_c$ and length $9\,nm$ reducing the reflectance $R_w < 0.1$ (Fig. 1a,c). That is almost all external power W is pumped into the resonator, where the electric field intensity of $|E_0|^2$ is increased Q times in respect to the pumped field. The resulting intensity enhancement G at the tip apex could be as large as $G \sim Q\varepsilon^2 a^6/(a^2 + b^2)^3 \gg 1$.

5. CONCLUSIONS

In conclusion, we propose to use the phenomenon of the resonance in the specially designed cascade dielectric structures to obtain strong field enhancement in a nanospot. Our NFT can be made from any transparent optically dense dielectric material. The huge field concentration is achieved without energy loss in the metal particles. For the practical application the two-dimensional design could be more preferable. Our computer simulations show that the dielectric edge, which is protruded from cylinder resonator, can also concentrate the em field. The designed systems could be used for heat assisted recording, nano sensing, local TERS and many other applications. Energy power released in a hotspot can be increased if the hotspot is a grain made of appropriate plasmonic material[18] possessing the surface resonance.

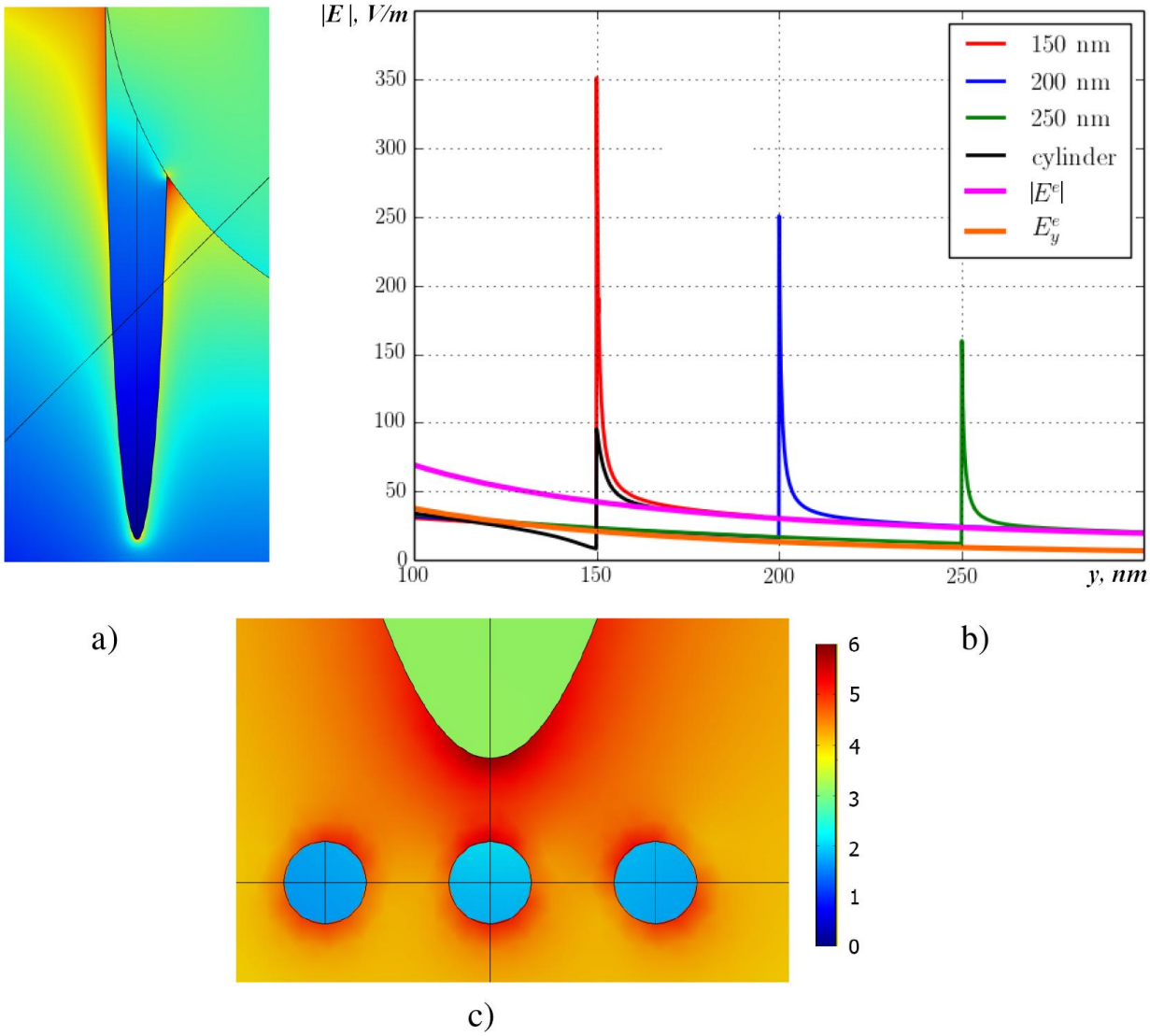

Figure 2. a) Dielectric tip guides electric field, $a = 111\,nm$, $\lambda = 900\,nm$; b) $|E|$–field profile along axis of the ellipsoidal tips of various length b, the apex curvature $R = 1\,nm$; external E^e–field and its tangent projection E^e_y in absence of the tip are also shown; note the internal field $|E|$ equals to applied field E^e_y, whereas it reduces near the end of cylindrical tip; c) tip heats $2\,nm$ nanoparticles made out of magnetic alloy FePt;[17] heat production inside central magnetic particle is 1.4 times larger than in its neighbors.

ACKNOWLEDGMENTS

We thanks the Supercomputing Center of the Novosibirsk State University for COMSOL computations; one of the authors (AKS) acknowledge important conversation with Prof. N. Boltasseva.

REFERENCES

1. A. Armani, R. Kulkarni, S. Fraser, R. Flagan, and K. Vahala, "Label-free, single-molecule detection with optical microcavities," *Science* **317**, pp. 783–787, 2007.
2. W. Challener, C. Peng, D. Itagi, A.V.and Karns, W. Peng, Y. Peng, X. Yang, X. Zhu, N. Gokemeijer, Y. Hsia, R. Rottmayer, and E. Seigler, M.A.and Gage, "Heat-assisted magnetic recording by a near-field transducer with efficient optical energy transfer," *Nature Photonics* **3**, pp. 220–224, 2009.

3. T. Aoki, B. Dayan, W. Wilcut, E.and Bowen, A. Parkins, T. Kippenberg, K. Vahala, and H. Kimble, "Observation of strong coupling between one atom and a monolithic micro-resonator," *Nature* **443**, pp. 671–674, 2006.
4. J. Schuller, E. Barnard, W. Cai, Y. Jun, J. White, and M. Brongersma, "Plasmonics for extreme light concentration and manipulation," *Nature Mat.* **9**, pp. 193–204, 2010.
5. L. Novotny and N. Hulst, "Antennas for light," *Nature photonics* **5**, pp. 83–90, 2011.
6. G. Yuan, E. Rogers, T. Roy, Z. Shen, and N. Zheludev, "Flat super-oscillatory lens for heat-assisted magnetic recording with sub-50nm resolution," *Opt. Exp.* **22**, pp. 6428–6437, 2014.
7. J. Bohn, D. Nesbitt, and G. A., "Field enhancement in apertureless near-field scanning optical microscopy," *JOSA A* **18**, pp. 2998–3006, 2001.
8. A. Bouhelier, M. Beversluis, A. Hartschuh, and L. Novotny, "Near-field second-harmonic generation induced by local field enhancement," *Phys. Rev. Lett.* **90**, pp. 013903 –4, 2003.
9. A. I. Kuznetsov, A. E. Miroshnichenko, Y. H. Fu, J. Zhang, and B. Luk'yanchuk, "Magnetic light.," *Scientific reports* **2**, p. 492, Jan. 2012.
10. M. Green, "Self-consistent optical parameters of intrinsic silicon at 300 k including temperature coefficients," *Solar Energy Materials and Solar Cells* **92**, pp. 1305 – 1310, 2008.
11. J. Bergmann, M. Heusinger, G. Andra, and F. F., "Temperature dependent optical properties of amorphous silicon for diode laser crystallization'," *Opt.. Exp.* **20**, pp. A856–A863, 2012.
12. E. Hallen, *Electromagnetic Theory*, Chapman and Hall, London, 1962.
13. C. Balanis, *Antenna Theory: Analysis and Design*, John Wiley, New York, 2005.
14. L. Cancado, A. Hartschuh, and L. Novotny, "Tip-enhanced raman spectroscopy of carbon nanotubes," *J. Raman Spectrosc.* **40**, pp. 1420–1426, 2009.
15. D. J. Bergman and M. I. Stockman, "Surface plasmon amplification by stimulated emission of radiation: Quantum generation of coherent surface plasmons in nanosystems," *Phys. Rev. Lett.* **90**, pp. 027402–5, 2003.
16. A. K. Sarychev and V. Shalaev, *Electrodynamics of Metamaterials*, World Scientific, 2007.
17. K. Sato, A. Mizusawa, K. Ishida, T. Seki, T. Shima, and K. Takanashi, "Magneto-optical spectra of ordered and disordered fept films prepared at reduced temperatures (magneto-optical effect and measurement)," *Trans. of the Magnetics Society of Japan* **4**, pp. 297 – 300, 2004.
18. P. R. West, S. Ishii, N. K. Naik, G. V. Emani, V. M. Shalaev, and A. Boltasseva, "Searching for better plasmonic materials," *Laser & Photonics Rev.* **4**, pp. 795–857, 2010.